THE JOURNAL OF BIOLOGICAL CHEMISTRY VOL. 286, NO. 40, pp. 35007–35019, October 7, 2011

Muscle Creatine Kinase Deficiency Triggers Both Actin Depolymerization and Desmin Disorganization by Advanced Glycation End Products in Dilated Cardiomyopathy*[S]

Received for publication, April 18, 2011, and in revised form, June 24, 2011 Published, JBC Papers in Press, July 17, 2011, DOI 10.1074/jbc.M111.252395

Nicolas Diguet[‡1], Youssef Mallat[‡], Romain Ladouce[‡], Gilles Clodic[§], Alexandre Prola[¶], Eva Tritsch[‡], Jocelyne Blanc[‡], Jean-Christophe Larcher[‖], Claude Delcayre[**], Jane-Lise Samuel[**], Bertrand Friguet[‡], Gérard Bolbach[§], Zhenlin Li[‡], and Mathias Mericskay[‡2]

From the [‡]Department of Aging, Stress and Inflammation, [§]IFR83 Mass Spectrometry Facility, [‖]CNRS UMR7622 Developmental Biology, UPMC University Paris 6, 75005 Paris, [¶]INSERM UMR-S 769 LabEx LERMIT University Paris-Sud 11, 92296 Châtenay-Malabry, and [**]INSERM U942, Biomarkers and Heart Diseases Université Denis Diderot Paris 7, 75010 Paris, France

Alterations in the balance of cytoskeleton as well as energetic proteins are involved in the cardiac remodeling occurring in dilated cardiomyopathy (DCM). We used two-dimensional DIGE proteomics as a discovery approach to identify key molecular changes taking place in a temporally controlled model of DCM triggered by cardiomyocyte-specific serum response factor (SRF) knock-out in mice. We identified muscle creatine kinase (MCK) as the primary down-regulated protein followed by α-actin and α-tropomyosin down-regulation leading to a decrease of polymerized F-actin. The early response to these defects was an increase in the amount of desmin intermediate filaments and phosphorylation of the αB-crystallin chaperone. We found that αB-crystallin and desmin progressively lose their striated pattern and accumulate at the intercalated disk and the sarcolemma, respectively. We further show that desmin is a preferential target of advanced glycation end products (AGE) in mouse and human DCM. Inhibition of CK in cultured cardiomyocytes is sufficient to recapitulate both the actin depolymerization defect and the modification of desmin by AGE. Treatment with either cytochalasin D or glyoxal, a cellular AGE, indicated that both actin depolymerization and AGE contribute to desmin disorganization. Heat shock-induced phosphorylation of αB-crystallin provides a transient protection of desmin against glyoxal in a p38 MAPK-dependent manner. Our results show that the strong down-regulation of MCK activity contributes to F-actin instability and induces post-translational modification of αB-crystallin and desmin. Our results suggest that AGE may play an important role in DCM because they alter the organization of desmin filaments that normally support stress response and mitochondrial functions in cardiomyocytes.

In the heart, ventricular chamber dilation is a common response to disorders that produce volume overload, such as what occurs following myocardial infarction. This distinct cardiac morphology also occurs in dilated cardiomyopathy (DCM),[3] a cardiomyopathy showing an important genetic contribution (1). Gene mutations that were identified in DCM occur essentially in extra-sarcomeric cytoskeleton proteins like lamin, desmin, and cytoskeletal linkers like vinculin or muscle lim protein, but also in sarcomeric proteins like actin (1), and in proteins involved in calcium signaling (2). One of the striking features of both acquired and genetic DCM is the eccentric remodeling of cardiomyocyte, *i.e.* an increase in the long axis without concomitant increase in the wide axis, and the stretching of the intercalated disks (ID), which connect cardiomyocytes in series and allow force transmission. These cytoarchitectural modifications are paralleled by a reorganization of the major filamentous cytoskeleton networks, including actin microfilaments, microtubules, and desmin intermediate filaments, each network being closely interconnected to the other, to the sarcolemma, and to organelles of the cardiomyocytes. These cytoskeletal networks are also intimately coupled to the bioenergetic structures, like mitochondria and the systems of energy transfer in the muscle cells like the phosphocreatine shuttle system (3).

The MADS box transcription factor serum response factor (SRF) is a major regulator of genes encoding contractile proteins, notably all muscle actin isoforms, but also of genes involved in energy transfer like muscle creatine kinase (MCK) or in calcium homeostasis like NCX1 (4). SRF is activated by cytokines, growth factors, and G-coupled receptors, which are known to play a major role in cardiac remodeling. SRF is also involved in regulatory feedback loops controlled by actin and titin cytoskeleton linked signals that adapt muscle gene expression to the work demand (5, 6). A few studies reported the presence of truncated forms of SRF in human heart failure (7, 8) and we showed that Cre-LoxP-mediated total or even partial

* This work was supported by "Agence Nationale pour la Recherche" Grants ANR-05-PCOD-003 and ANR-08-GENOPAT-038 and the "Association Française contre les Myopathies" (AFM).

[S] The on-line version of this article (available at http://www.jbc.org) contains supplemental Tables S1 and S2 and Figs. S1–S7.

[1] Supported by a Ph.D. fellowship from the French Ministry of Research and AFM.

[2] To whom correspondence should be addressed: Université Pierre et Marie Curie Paris 6, UR4 Vieillissement, Stress, Inflammation 7, quai Saint Bernard, BP 256, 75005 Paris, France. Tel.: 33-1-4-27-26-45; Fax: 33-1-44-27-21-35; E-mail: mathias.mericskay@upmc.fr.

[3] The abbreviations used are: DCM, dilated cardiomyopathy; AGE, advanced glycation end products; DIGE, differential in gel electrophoresis; FC, fold-change; ID, intercalated disk; HS, heat shock; MCK, muscle creatine kinase; SRF, serum response factor; SRF^{HKO}, SRF heart knockout; LV, left ventricle; NRC, neonatal rat cardiomyocyte; TRITC, tetramethylrhodamine isothiocyanate; D25, D45 etc., days after tamoxifen injection.

inactivation of the SRF gene in the adult mouse heart leads to actin polymerization defects, cardiac chamber dilation, and heart failure (9, 10). Altogether, these studies strongly suggest that alterations of SRF activity could be involved in the pathogenesis of both genetic and acquired DCM and heart failure.

The inducible SRF heart knock-out (SRF^{HKO}) mice develop a progressive DCM within an experimentally controlled time frame (9). We took advantage of this unique experimental setting to adopt a proteomic discovery approach to identify the key markers of disease progression that could play a role in the pathogenesis of DCM. Here we characterize a temporal cascade of molecular events going from early down-regulation of MCK to actin polymerization defect, triggering the recruitment of phosphorylated αB-crystallin at sites of deficient F-actin to the detriment of another major αB-crystallin client protein, the desmin intermediate filament. Finally, we show that desmin is a preferential target of advanced glycation end products (AGE) that lead to the disorganization of this essential cytoskeletal lattice connecting myofibrils to mitochondria and sarcolemma.

EXPERIMENTAL PROCEDURES

SRF^{HKO} Mouse Model—SRF^{HKO} mice homozygous for the *Srf*-floxed allele (Sf) bearing one copy of the tamoxifen-inducible α-MHC-MerCreMer transgene have been described previously (9). The α-MHC-MerCreMer transgenic mice were a kind gift of Dr. J. Molkentin (University of Cincinnati) (11). The mice used for the present study have been backcrossed with C57BL/6J mice for at least 20 generations. Groups of 2-month-old (α-MHC-MerCreMer:Sf/Sf) and control (Sf/Sf) male mice were given daily intraperitoneal tamoxifen (20 mg/kg/day; Sigma) injections on 3 consecutive days, with the day of the first injection counted as day 0. This study conformed to institutional guidelines for the use of animals in research.

Patients—Studies were performed with left ventricular myocardium (LV) from controls ($n = 3$) and end-stage failing hearts from patients with idiopathic dilated cardiomyopathies ($n = 7$). The clinical data of patients have been described previously (12). Briefly, patients presented increases in LV mass and decreased LV ejection fraction (14 ± 5%). This study was approved by the Consultative Committee for the Protection of Human Subjects in Biomedical Research (Paris, France).

Left Ventricular Tissue Preparation for Use in Proteomic and Biochemical Analyses—For all proteomic and biochemical experiments, 2-month-old α-MHC-MerCreMer:Sf/Sf and control (Sf/Sf) mice were sacrificed at 25 (D25) or 45 (D45) days after tamoxifen injection. Male mice were used to eliminate gender effect when comparing the protein profiles of SRF mutant and control hearts. Directly following euthanasia, the LV was excised, blotted, and frozen in liquid nitrogen. Frozen tissue was subsequently powdered in a percussion mortar cooled in liquid nitrogen.

Two-dimensional Gel Electrophoresis, Gel Staining, Image Acquisition—Powdered LV tissue was dissolved in 15 volumes (μl/mg of tissue powder) of lysis UTC buffer (8 M urea, 2 M thiourea, 4% CHAPS, 50 mM DTT). The crude extract was homogenized using a syringe and needle (21 gauge) and centrifuged at 20,000 × *g* for 30 min at 15 °C, and the supernatant was precipitated using a two-dimensional clean-up kit (GE Healthcare) following the manufacturer's recommendations. Protein pellets were dissolved in lysis buffer without DTT. Protein concentration was determined using Bradford assay (Bio-Rad). To screen for protein amount differences and obtain quantitative protein ratios, Two-dimensional Differential In Gel Electrophoresis (DIGE) was performed on four paired samples (4 SRF mutant and 4 WT) for each experiment. Control and mutant heart protein extracts (50 μg) were labeled with the CyDye DIGE Fluor minimal labeling kit (GE Healthcare) following the manufacturer's recommendations. An internal standard was made by mixing equal amounts of proteins from each sample and labeled with Cy2. For analytical gels, 18-cm Immobiline DryStrip gels (pH 3–11NL (nonlinear)) were loaded with a total protein amount of 150 μg (50 μg of each control and mutant extract and 50 μg of internal standard). For preparative gels, we used 450 μg of pooled control or mutant unlabeled protein extracts. Strips were rehydrated overnight in the presence of proteins in a volume of 350 μl of rehydration solution (8 M urea, 2 M thiourea, 2% CHAPS, 1.2% DeStreak Reagent, 0.5% IPG buffer pH 3–11NL. Isoelectric focusing was performed with an Ettan IPGphor2 apparatus (GE Healthcare) at 150 V for 6 h, followed by stepwise application of 200, 1000, and 8000 V for a total of 35,000 V-h. After focusing and equilibration, strips were applied to 8–18% gradient SDS-PAGE gels and sealed with 1% agarose, containing bromphenol blue. Electrophoresis was performed at 20 °C in an Ettan DALT-6 tank with electrophoresis buffer (25 mM Tris, pH 8.3, 192 mM glycine, and 0.2% SDS) for a total of 2,000 V-h. For each experiment, 4 analytical and 2 preparative gels were run in parallel. Analytical gels were imaged using an Ettan DIGE imager (GE Healthcare) scanner. Data were analyzed with DeCyder 7.0 software (GE Healthcare) using the batch process mode. An unpaired Student's *t* test was used to determine the statistical difference of the mean ratio between control and mutant groups. Unlabeled preparative gels were fixed and stained with Coomassie Brilliant Blue G-250 for 5 days and scanned with the Ettan DIGE imager using the Cy5 channel. Matching the protein spots of interest between analytical and preparative gels was performed manually.

MS and MS-MS Analysis—In-gel digests were purified with homemade microcolumns packed with Poros reversed-phase 20 R2 resin (Applied Biosystems) using GELoader tips (Eppendorf) as described previously (13, 14). The Poros 20 R2 column was washed with 20 μl of 0.1% TFA, and the bound peptides were eluted directly onto the MALDI target using 0.5 μl of a matrix solution consisting of α-cyano-4-hydroxycinnamic acid (5 mg/ml) in 50% acetonitrile, 0.1% TFA. Typically, 1–10 μl of digest were purified. Matrix-assisted laser/desorption ionization-time-of-flight (MALDI-TOF) mass spectrometry was performed on a 4700 Proteomics Analyzer (Applied-Biosystems).

MALDI-TOF (MS) positive ion mass spectra of the samples were performed in reflector mode and delayed extraction using m/z 2100, near the threshold fluence. MALDI-TOF-TOF (MS-MS) experiments were carried out with and without gas for the study of fragmentation through metastable decomposition and CID with gas (N2, 2×10^{-7} torr) with collision energy of 1 keV, respectively. For MALDI-TOF-TOF experiments, the precur-

sor ion window was adjusted to be certain of the correct selection. MS and MS-MS spectra were recorded by averaging a few hundred to a few thousand laser shots allowing a significant isotopic pattern of peptides and fragment ions. MALDI-TOF and MALDI-TOF-TOF spectra were calibrated using classic peptide standards (Applied Biosystems). Data Explorer 4.6 software was used to analyze the MS and MS-MS spectra and to generate the peak lists (MS or MS and MS-MS data), which were submitted to data base search program MASCOT (Matrix Science, UK). Parameters for protein identification by MS included: a mass tolerance of 75 ppm, a maximum of two missed trypsin cleavages per peptide, and the acceptance of carbamidomethylation of cysteines and oxidation of methionines. For protein identification with MS-MS data, the mass tolerance was set to 0.1 Da and the charge state +1 using SwissProt as the main data bank. Positive identifications depended on a MOWSE score (molecular weight search algorithm) of around 40, the location of missed cleavages and whether significant peaks in the MS spectra were those used for the analysis. Finally, both the molecular weight (M_r) and isoelectric point (pI) of each data base-matched protein were compared with those of the sample by referring to its position on the two-dimensional gels.

Measurement of CK Activity and ATP—Frozen tissue samples were weighed, homogenized in ice-cold buffer (50 mg wet weight per ml) containing: 5 mM HEPES (pH 8.7); 1 mM EGTA; 1 mM dithiothreitol; and Triton X-100 (0.1%), and incubated for 60 min at 4 °C for complete enzyme extraction. CK activity was measured spectrophotometrically with the coupled-enzyme system using hexokinase and GAPDH in the presence of phosphocreatine (10 mM) and ADP (1.2 mM). The appearance of NADPH was followed at 340 nm. Isoforms are separated by nondenaturating electrophoresis and revealed by enzymatic activity to measure the percentage of each isoform. ATP and ADP/ATP ratios were measured using the bioluminescent ADP/ATP ratio assay kit from Abcam as indicated by the manufacturer with minor modifications. Briefly, cardiac tissue was frozen in liquid nitrogen and powdered with a mortar. Tissue powder was suspended in the provided lysis buffer (10 μl/mg of tissue powder) for 5 min exactly at room temperature, followed by centrifugation at 10,000 $\times$ *g* for 1 min to pellet insoluble material. We used 50 μl of supernatant per assay in a final volume of 100 μl. Luciferase units were converted to picomoles of the amount of ATP by plotting against a standard curve with serial dilution of ATP. Data were normalized by the amount of protein present in the supernatant as measured by the Bradford assay.

Western Blot Analysis—One-dimensional and two-dimensional PAGE were carried out as described previously (15, 16). Proteins were transferred onto nitrocellulose membranes (Hybond C, Amersham Biosciences) and the blots were saturated in TBS-T buffer (20 mM Tris, pH 7.5, 136.8 mM NaCl, and 0.1% (v/v) Tween 20) containing 5% (w/v) low fat milk. The following primary antibodies were used for Western blot: mouse monoclonal anti-sarcomeric α-actin (1:400, Sigma, recognize both cardiac and skeletal α-actin), mouse monoclonal anti-α-tropomyosin, rabbit polyclonal anti-GAPDH (1:400, Santa Cruz), rabbit polyclonal anti-Histone-3 (1:400, Sigma), mouse monoclonal anti-αB-crystallin (1:200, Abcam), and anti-phosphorylated serines 19, 45, and 59 on αB-crystallin (1:500, StressGen). Polyclonal anti-AGE antibody was a kind gift of Dr. Bakala and has been previously characterized (17, 18). It recognizes a variety of AGE products such as carboxymethyl lysine and carboxyethyl lysine. Polyclonal anti-4-hydroxy-2-nonenal lipid peroxidation product recognizes 4-hydroxy-2-nonenal adducts with lysine, cysteine, and histidine within proteins and were generated as originally described (19). The protein oxidation detection kit, OxyBlot, was purchased from Chemicon (Millipore).

HRP-conjugated secondary anti-rabbit (1:5,000) or anti-mouse (1:5,000) antibody (Dako) was used to detect the proteins by ECL. For Western blot with anti-phospho-Ser αB-crystallin antibodies, heart tissue proteins were extracted in anti-phosphatase buffer (20 mM MOPS, pH 7.2, 0.5% Nonidet P-40, 2 mM EGTA, 5 mM EDTA, 30 mM NaF, 40 mM sodium pyrophosphate, 1 mM $NaVO_4$, protease inhibitor mixture (Roche Applied Science), 1 mM PMSF). For all other Western blots, cardiac protein extracts in urea/thiourea/CHAPS buffer were the same as used for two-dimensional DIGE. For Western blot analyses of cultured cardiomyocytes, proteins were harvested in either UTC buffer, except for cell fractionation. For fractionation experiments, proteins were extracted in RIPA buffer (150 mM NaCl, 5 mM EDTA, 1% Tween 20, 50 mM Tris, pH 7.4, protease inhibitor mixture (Roche Applied Science)), incubated for 30 min on ice, and then centrifuged for 1 h at 20,000 $\times$ *g*. The supernatant was from the soluble fraction containing G-actin. Pellets were dissolved in UTC buffer to extract cytoskeletal proteins including F-actin.

Isolation and Treatments of Neonatal Rat Cardiomyocytes—1-day-old rat pups were killed by decapitation and the cardiac ventricles were harvested and minced into 1 to 2-mm wide cubes with scissors. After washing with Tyrode solution, heart fragments were subjected up to 10 rounds of digestion with 0.05 mg/ml of Liberase Blendzyme 4 (Roche Applied Science) in oxygenated Tyrode solution under agitation. The supernatant of the first digestion was discarded and the following digestion was stopped in DMEM, 10% FCS. Cultures were enriched in cardiomyocytes by centrifugation in a discontinuous Percoll gradient (bottom 58.5%, top 40.5%, 30 min, 3000 rpm). Neonatal cardiomyocytes were seeded at a density 5×10^5 cells/well in 6-well plates on coverslips coated with 10 μg/ml of laminin (BD Biosciences) in DMEM, 10% horse serum, 5% FCS and cultured at 37 °C in 1% CO_2 atmosphere. For siRNA transfections, Rn_Ckm_2 siRNA (SI01499190), Rn_Tpm1_1 siRNA (SI02047507), and negative control siRNA (SI03650325) from Qiagen were transfected at 10 nM final concentration using RNAiFect (Invitrogen) from day 5 to 8. For phosphocreatine shuttle inhibition, cells were cultured in the presence of 10 mM β-guanidinopropionic acid between days 3 and 8 in the presence of 20 μM phenylephrine to increase energy expenditure in culture. For heat shock experiments, 6-day cell cultures were maintained at 42 °C for 30 min. Cytochalasin D (20 μM) or glyoxal (10 mM) were added to the medium and the cells were decreased to 37 °C for 30 min. When the p38 MAPK inhibitor SB202190 (20 μM) was used, it was added to the medium 6 h before heat shock treatment.

Immunofluorescence—Immunofluorescence stainings were done on frozen heart sections or isolated cardiomyocytes with the following primary antibodies: TRITC-coupled phalloidin (1:100, Fluka), mouse monoclonal anti-desmin (1:50, D33, Dako), mouse monoclonal anti-αB crystallin (1:1000, Abcam), rabbit polyclonal anti-phospho-Ser^{45} and Ser^{59} αB crystallin (1:100, StressGen), followed by Cy3-coupled secondary antibodies (1:400, Jackson ImmunoResearch) or Alexa 488 or 633 coupled secondary antibodies (1:400, Invitrogen).

Desmin Striation Pattern—To estimate in an unbiased manner the degree of striation from the desmin signal pattern, we acquired the desmin signal intensity profile along a parallel line to alignment of the main axis of phalloidin-stained F-actin filaments in at least 5 cardiomyocytes for each condition, using ImageJ software. Data were processed using the fast Fourier transform function in Microsoft Excel using the signal along a distance in pixels equal to a power of 2 as requested (128 pixels = 35 μm, in the central region of the cardiomyocyte). We obtained a series of spectra giving the sinusoid amplitude (A) as a function of spatial frequency (pixels were converted to μm^{-1} based on the scale of magnification). Data are shown as an average spectrum for each group ± S.E.

Statistical Analysis—The data are expressed as mean ± S.E. An unpaired Student's *t* test was used to determine the probability value (*p* value). A *p* value ≤ 0.05 was considered statistically significant.

RESULTS

Proteomic Changes in the SRF-deficient Dilated Heart—Adult mice deficient for SRF in the cardiomyocytes of the heart (SRF^{HKO}) develop a progressive reduction of ejection fraction starting around 3 to 4 weeks after SRF gene inactivation followed by dilation of all cardiac chambers and overt heart failure and death around D60–65 after gene inactivation (9). So, D25 was established as an early stage in disease progression at the beginning of the alterations of cardiac functions and D45 was established as a model of intermediate stage-dilated cardiomyopathy for our subsequent proteomics analyses. To identify differentially expressed proteins, we prepared whole left ventricle proteins from control and mutant hearts at each time point and performed two-dimensional DIGE analyses at D25 and D45 (Fig. 1*A*). Detailed quantitative analyses and protein identification data are provided under supplemental Tables S1 and S2. Whole tissue protein preparations revealed an average of 1900 unique protein spots at each time point. Principal component analysis using all matched spots separated the control and mutant samples at D45 but not at D25 (supplemental Fig. S1). The two-dimensional DIGE analysis identified 16 protein spots significantly altered ($p \leq 0.05$, fold-change (FC) ≥ 1.3) at the early stage (D25) and 118 spots at the intermediate stage (D45) using the same criteria. We identified 45 protein spots by MALDI-TOF peptide analysis and validated 29 spots by MALDI-TOF-TOF peptide fragmentation, representing altogether 33 unique proteins (Fig. 1*A* and supplemental Tables S1 and S2).

Early Down-regulation of MCK and Loss of Polymerized Actin in the SRF^{HKO}—At D25, when the heart of SRF^{HKO} mice is just starting to show signs of reduced contractility, the proteomic screen indicated that MCK was the most down-regulated protein (FC −2.02, $p = 3.8E-05$, supplemental Table S1). Quantitative RT-PCR analysis showed a strong down-regulation of MCK mRNA as soon as D15 in agreement with the fact that the *Ckm* gene encoding MCK is a direct target of SRF (supplemental Fig. S2). In accordance with results of the proteomic screen, the ventricular muscle of the SRF^{HKO} mutant at D25 demonstrated a significant decrease of total CK activity that could be attributed exclusively to a 50% loss of MCK MM-dimer activity without changes in mitochondrial CK and brain cytosolic CK activity (Table 1). At D45, we observed a down-regulation of several mitochondrial enzymes involved in fatty acid β-oxidation and of β-enolase, a major enzyme in muscle gycolysis, and further down-regulation of MCK (FC −5.8, $p = 1.3E-07$, supplemental Table S1). Measurement of the ATP amount in the myocardial tissue at D45 showed a significant reduction in the SRF^{HKO} heart (SRF^{HKO} 5.5 ± 1.6 *versus* controls, 15 ± 3.4 pmol/mg of protein; pval = 0.044, $n = 6$ each group). Accordingly the ADP/ATP ratio was raised in the SRF^{HKO} heart (SRF^{HKO} 2.74 ± 0.62 *versus* controls, 0.82 ± 0.28; pval = 0.014). Altogether, these results show that energy reserve is altered in the failing SRF-deficient heart as in most models of heart failure (20). Up-regulation of AK1 and ATP-synthase subunit d likely reflects an attempt of compensatory response to maintain ATP synthesis (supplemental Tables S1 and S2).

Two sarcomeric proteins, troponin-T and –I, were down-regulated at D45 (supplemental Table S1). In addition, sarcomeric α-actin and α-tropomyosin were down-regulated albeit only by a factor 1.2 at D45 (supplemental Table S2). The low FC value for these proteins in two-dimensional DIGE may be explained by saturation of the cyanine signal for these abundant proteins. The cardiac and skeletal α-*Actin* genes that encode sarcomeric actins and the *Tpm1* gene encoding α-tropomyosin were strongly down-regulated at an early stage as expected from being direct SRF targets (supplemental Fig. S2). Western blot analyses, however, showed a minor reduction of these 2 proteins at D25 and only 50% reduction at D45; highlighting the long half-life of these proteins *in vivo* (Fig. 2*A*). Yet, the polymerization state of the actin filament was strikingly already altered at D25 in isolated cardiomyocytes as shown by the 50% decrease in the F-actin-specific phalloidin signal accompanying the beginning of exocentric remodeling at this stage (Fig. 2, *C*, *D*, *F*, *G*, and *I*). Interestingly, cytoskeletal β-actin, which has been shown to play an important role in ID structure (21), was up-regulated in the SRF^{HKO} heart and localized in the subsarcolemal domain as well as connecting the last sarcomere to the stretched ID, in an apparent attempt to cope for sarcomeric actin down-regulation (Fig. 2, *B*, *E*, and *H*).

Up-regulation and Post-translational Modification of αB-Crystallin and Desmin in the SRF-deficient Cardiomyocytes—In parallel to the reduction in energy metabolism and sarcomeric proteins, there was a significant increase in stress response proteins including αB-crystallin and heat shock proteins HSP90β, HSP70, and HIP. Likewise, cytoskeletal proteins including desmin as well as tubulin β-2C and Csrp3/MLP (cysteine and glycine-rich protein 3/muscle lim protein) were increased. Among the up-regulated proteins, αB-crystallin and desmin were the only markers to be up-regulated at D25 sug-

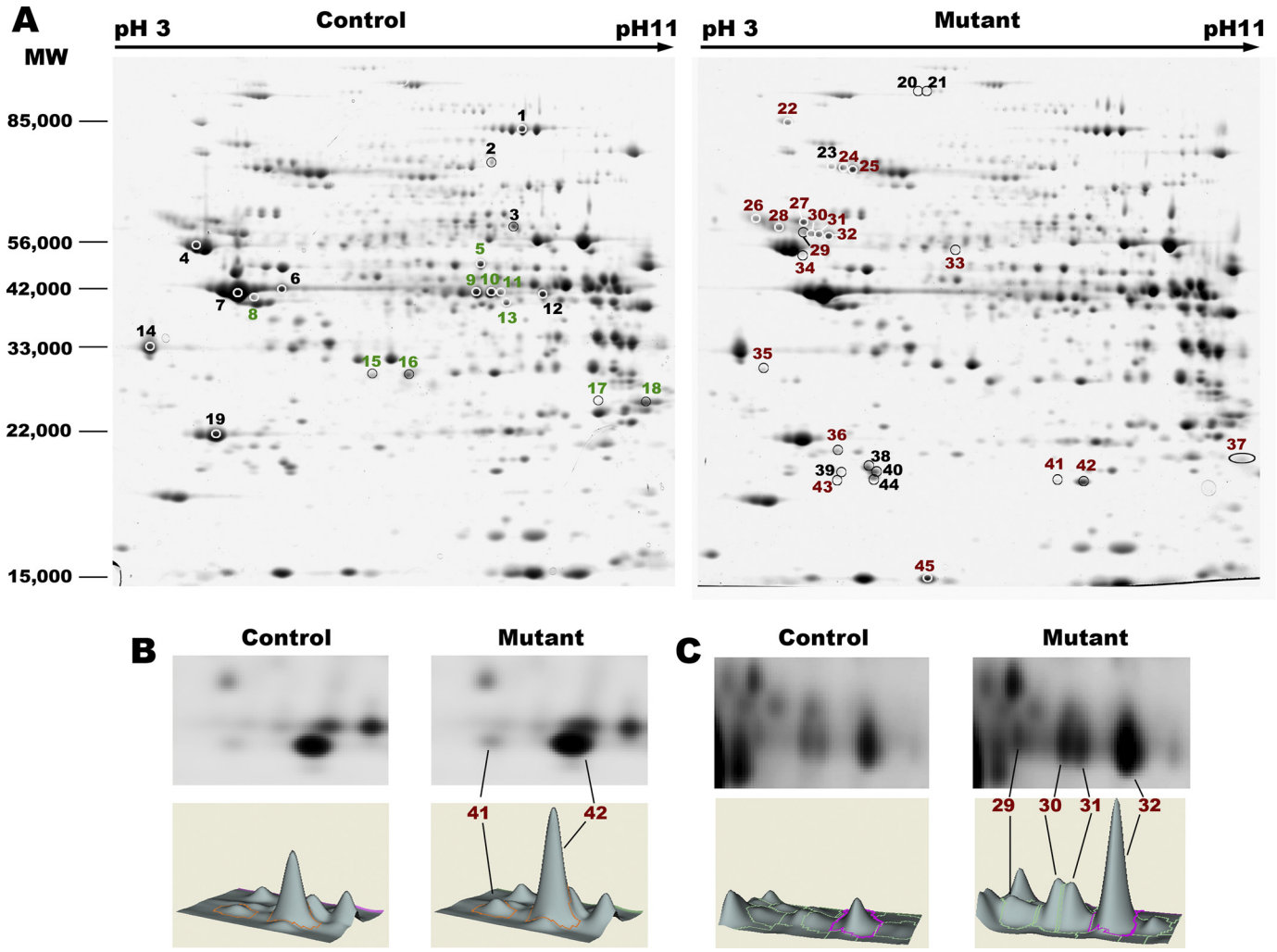

FIGURE 1. **Two-dimensional DIGE analysis of cardiac proteins from controls and SRF^{HKO} mice.** *A*, Coomassie Brilliant Blue-stained two-dimensional gels used for spot identification by MALDI-TOF/TOF. Whole ventricular protein preparations were separated by isoelectric focusing (Immobiline DryStrip gels pH 3–11NL) and apparent molecular weight (nominal range 15,000 to 100,000). Down-regulated spots (*green*) and up-regulated spots (*red*) were indicated on control (*left*) and mutant gels (*right*), respectively, and are listed under supplemental Table S1. Additional spots identified by MS only and/or with low FC (*black*) are listed under supplemental Table S2. *B* and *C*, Decyder 7.0 visualization of cyanine-labeled spots and three-dimensional spot volumes: (*B*) αB-crystallin spots at day 25; (*C*) desmin spots at day 25. Images are representative of $n = 4$ gels.

TABLE 1

CK isoenzyme profile of activity in control and SRF^{HKO} mice at D25

Values are in IU per g of ventricle dry weight (MM, MCK dimer activity; MB, MCK-BCK heterodimer; BB, BCK homodimer; sMitCK, sum of sMitCK dimer and octamer activity).

	Total CK	MM	MB	BB	sMit CK
Control ($n = 6$)	1818 ± 124	1270 ± 54.4	62 ± 10.5	56 ± 11	430 ± 70.2
SRF^{HKO} ($n = 6$)	1122 ± 90[a]	593 ± 34.2[b]	51 ± 12.6	62 ± 14.7	416 ± 72.5

[a] p value = 1.1.E-3.
[b] p value = 1.E-6.

gesting they are the first responders to the thin filament and MCK defect (supplemental Table S1).

This up-regulation occurred at the post-transcriptional level because corresponding mRNAs were not increased in the SRF mutant (supplemental Fig. S2). Spots 41 and 42 migrating at different pI but identical apparent M_r were identified as αB-crystallin suggesting post-translational modification such as phosphorylation (Fig. 1*B*). In agreement with this hypothesis, we detected phosphorylation on serine 45 and 59 of αB-crystallin that was significantly increased as soon as D25 (Fig. 3). The level of serine 19 phosphorylation was not modified (data not shown). Increased phosphorylation on serines 45 and 59 has been associated with recruitment on cytoskeletal components (22, 23).

For desmin, DIGE analysis showed the presence of four spots migrating at different pI but identical apparent M_r that were all up-regulated with a FC ranging from 2.49 to 2.88 (Fig. 1*C* and supplemental Table S1). The increase of desmin was confirmed by Western blot analysis (Fig. 4*A*).

MS and MS-MS analysis revealed the presence of a m/z 2158.08 peptide compatible with a single phosphorylation (+80 Da) of the m/z 2078.11 peptide (residues 17–37) in desmin spots 29, 30, and 31 but not in the basic spot 32. MS-MS fragmentation of m/z 2158.08 peptide revealed that the phosphate group was added to serine 28 (supplemental Fig. S3). Sequential two-dimensional Western blot analysis with anti-phosphoserine residues followed by anti-desmin antibody showed that the acidic desmin spots did contain phosphoserines (Fig. 4*B*), although the main basic spot equivalent to spot 32 was also

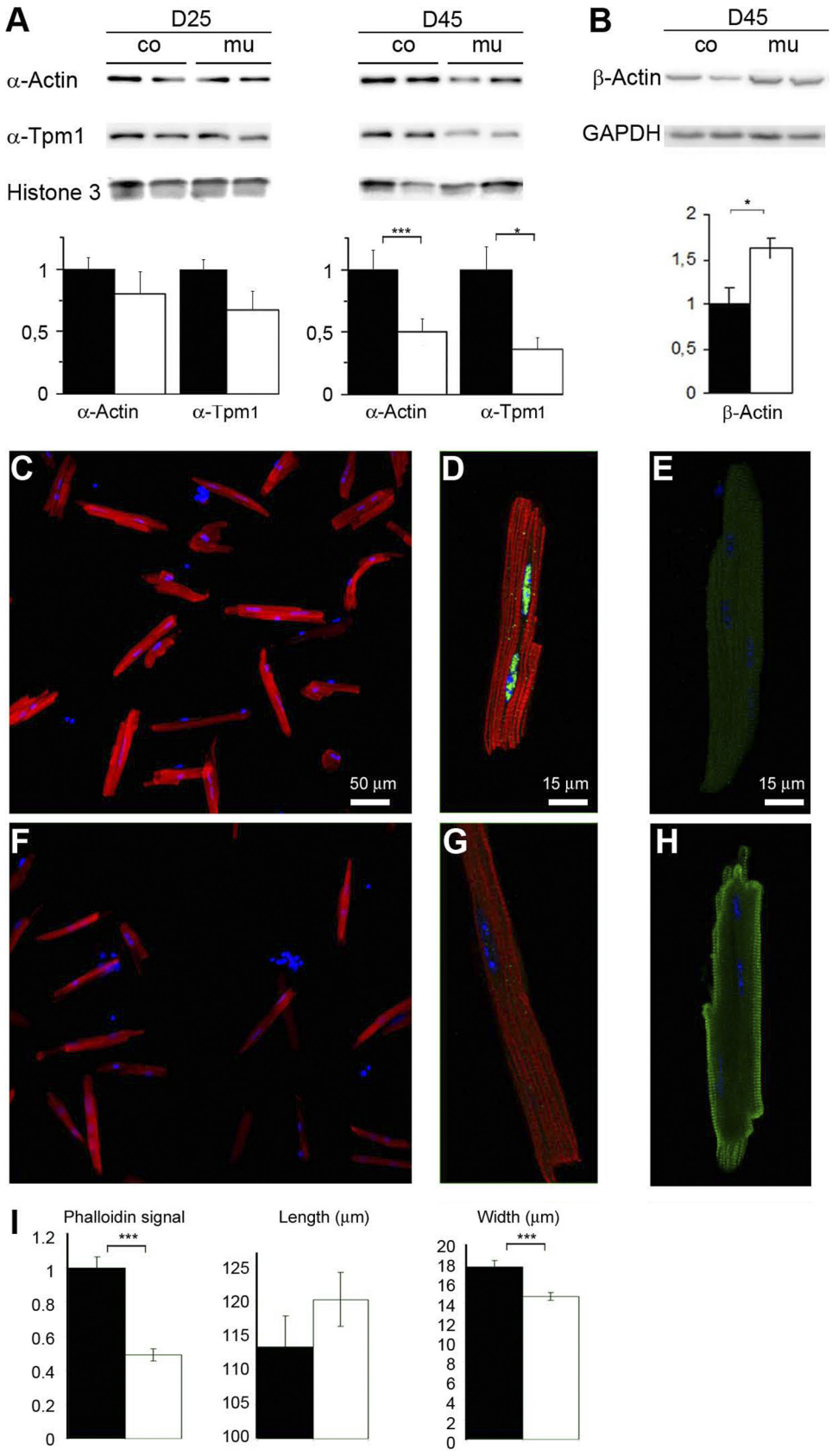
A
D25
co
mu
D45
co
mu
α-Actin
α-Tpm1
Histone 3
1
0,5
0
***
*
α-Actin
α-Tpm1
α-Actin
α-Tpm1
B
D45
co
mu
β-Actin
GAPDH
2
1,5
1
0,5
0
*
β-Actin
C
50 µm
D
15 µm
E
15 µm
F
G
H
I
Phalloidin signal
1.2
1
0.8
0.6
0.4
0.2
0
***
Length (µm)
125
120
115
110
105
100
Width (µm)
20
18
16
14
12
10
8
6
4
2
0
***

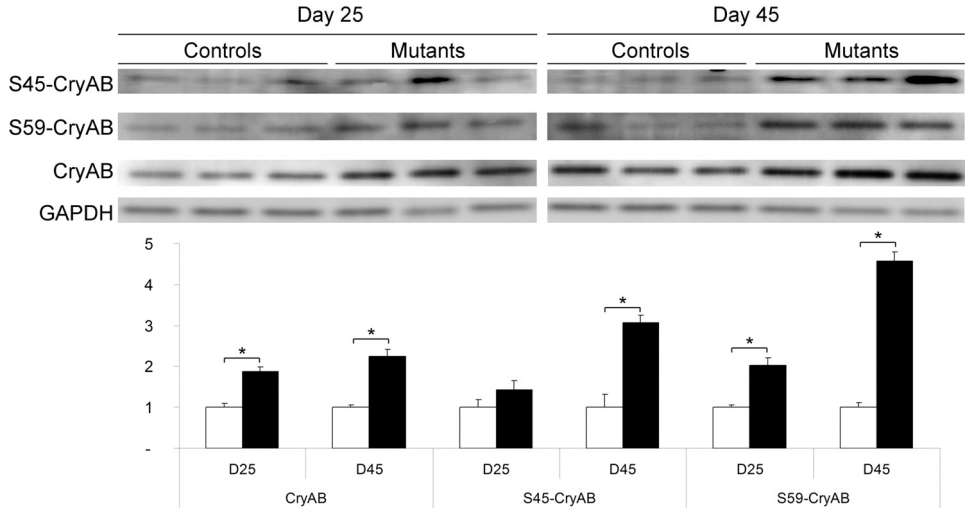

FIGURE 3. **Induction of phosphorylation on αB-crystallin in SRF^{HKO} hearts.** *Upper panel*, Western blot analysis of control and mutant hearts at D25 and D45 with anti-αB-crystallin (*CryAB*), -phospho-Ser^{45}-CryAB, -phospho-Ser^{59}-CryAB, and -GAPDH antibodies. *Lower panel*, quantification of Western blot ($n = 3$ for each group). Band intensities are normalized on GAPDH as a loading control. Ratios are expressed as fold-change over mean control value ± S.E. □, control; ■, SRF^{HKO}. *, $p \leq 0.05$.

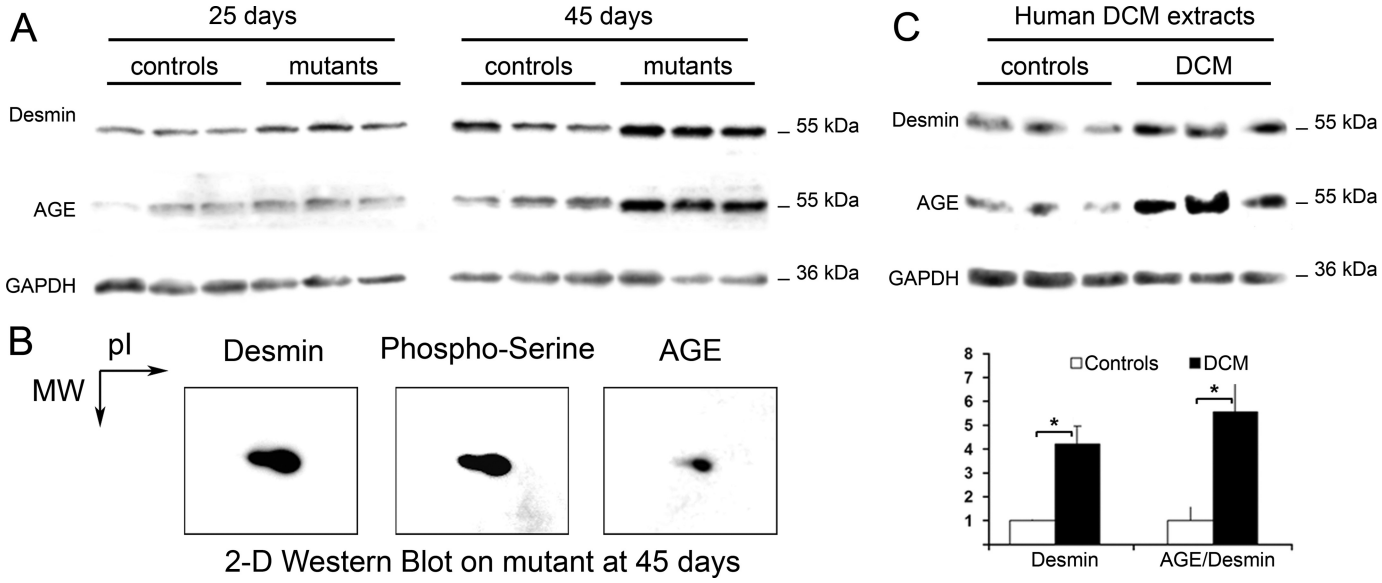

FIGURE 4. **AGE formation on desmin in SRF^{HKO} induced DCM and human DCM.** *A*, one-dimensional Western blot analysis of cardiac protein extracts from SRF^{HKO} with anti-desmin, -AGE, and -GAPDH antibodies. *B*, two-dimensional Western blot of anti-desmin, -phosphoserine, and -AGE antibodies at D45 after SRF inactivation. *C*, *upper panel*: Western blot on human DCM extracts with anti-desmin, -AGE, and -GAPDH antibodies. *Controls,* extracts from normal human ventricles; *DCM,* heart extracts from patients with dilated cardiomyopathy. *Lower panel*, quantification of desmin/GAPDH ratios and AGE/desmin ratio of control ($n = 3$) and patient ($n = 7$). □, control; ■, DCM. *, $p \leq 0.05$.

labeled, suggesting that serine residues other than serine 28 are also phosphorylated.

Desmin Is Modified by Advanced Glycation End Products in SRF^{HKO} Dilated Hearts and Human Patients with DCM—We assayed other types of post-translational modifications (supplemental Fig. S4). Oxidative stress as estimated from the oxiblot assay was increased in the SRF^{HKO} heart at D45, whereas the anti-4-hydroxy-2-nonenal lipid peroxidation product did not show major changes. Anti-AGE polyclonal antibody revealed a significant increase in the intensity of a band migrating at an apparent molecular mass of 55-kDa at D45 (Fig. 4*A* and supplemental Fig. S4). This band overlapped with the desmin band in the same blot (Fig. 4*A*). Sequential two-dimensional Western blot with anti-desmin and anti-AGE antibodies con-

FIGURE 2. **Reduced actin level and polymerization in the SRF^{HKO} cardiomyocytes.** *A*, slow progressive reduction of sarcomeric α-actin and α-tropomyosin 1 (α-*Tpm1*) detected by Western blot analysis of cardiac tissue cytoskeletal extracts (5 μg/lane) at D25 and D45. β-Actin is increased at D45. Loading controls: histone-3 and GAPDH. *Right*, quantification of band intensities normalized on loading controls. Data are expressed as fold-change over mean control value ± S.E. *B*, *C*, *E*, and *F*, immunofluorescent labeling of cardiomyocytes isolated from control (*B* and *C*) and SRF^{HKO} hearts at D25 (*E* and *F*) with TRITC-phalloidin (*red*) and SRF antibody (*green*). *C* and *F,* higher magnification of representative cardiomyocytes from each genotype. Note the presence of SRF in nuclei of control cardiomyocytes in *C*. *D* and *G*, immunofluorescent labeling of controls (*D*) and SRF^{HKO} hearts at D25 (*G*) with β-actin in *green*. *I*, quantification with ImageJ of the phalloidin fluorescent signal (integrate intensity), cardiomyocytes length, and width (μm). $n = 30$ for each group. Data are given as mean ± S.E. □, control; ■, SRF^{HKO}. *, $p < 0.05$; ***, $p < 0.001$. *Scale bar*, 50 μm in *B* and *D*, 15 μm in *C* and *E*.

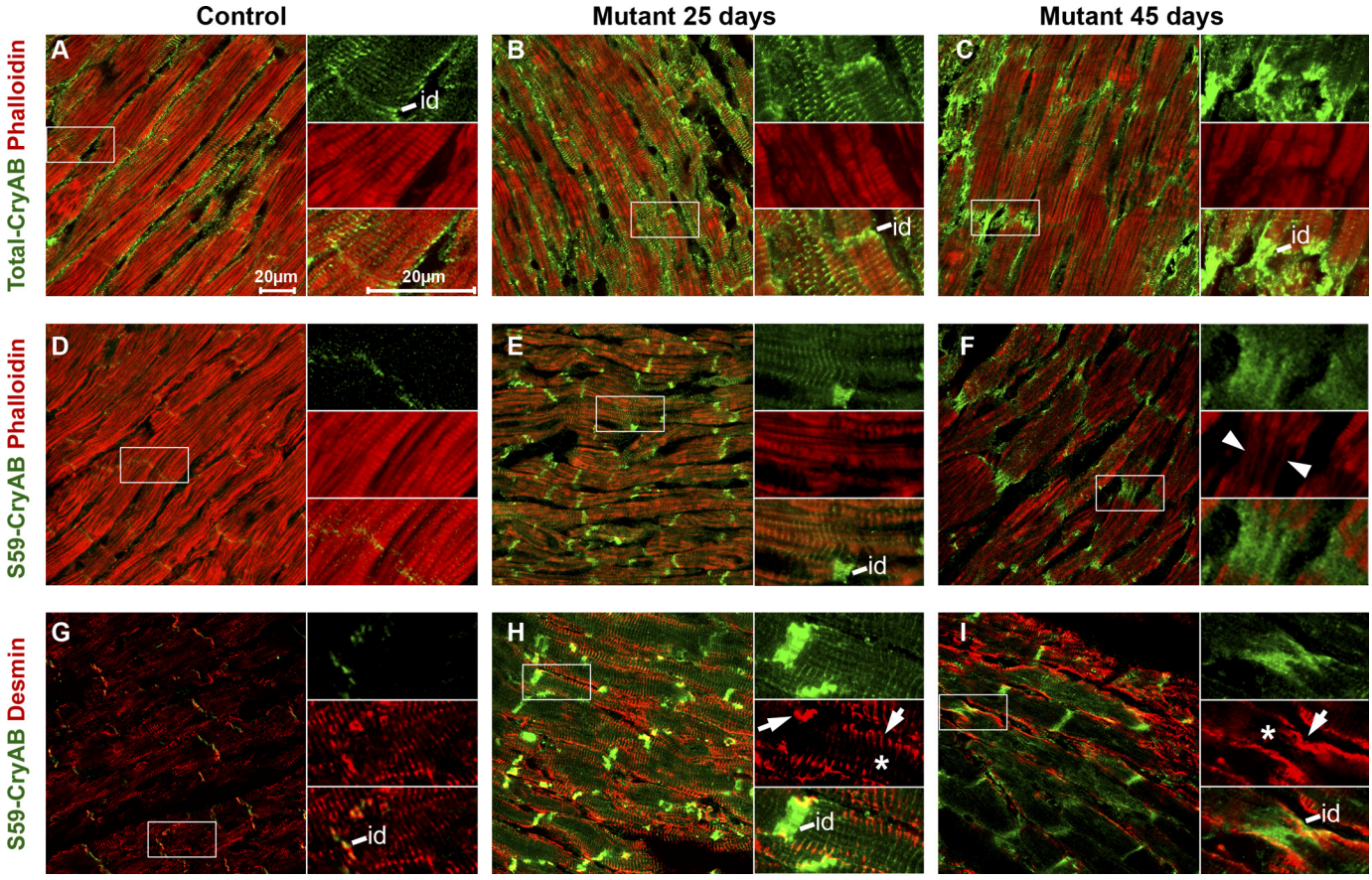

FIGURE 5. **Changes in αB-crystallin and desmin localization in SRF^{HKO} cardiomyocytes.** Immunofluorescent co-staining for total αB-crystallin (*CryAB*) (*A–C*) or phospho-Ser^{59} CryAB (*D–I*) in *green* and F-actin using phalloidin-TRITC (*A–F*) or desmin (*G–I*) in *red* on heart cryosections at D25 and D45. *A*, *D*, and *G*, control; *B*, *E*, and *H*, mutant D25; *C*, *F*, and *I*, mutant D45. *Right insets*, higher magnification of the *boxed* area with separate channels and merged picture. Total CryAB increases at D25 (*B*) both on actin filaments in the sarcomeres and at the level of intercalated disks (*id*) when actin starts to depolymerize. At D45 (*C*) total CryAB is mainly increased at the ID although the signal is still detected at the level of the Z-disk (*right inset*). *D*, phospho-Ser^{59} CryAB signal is weakly detected at the ID in the control (*D*) but increases strongly in both the sarcomere and ID at D25 (*E*). Phospho-Ser^{59} CryAB is detected only in ID at D45 (*F*) where it colocalizes with weakly stained actin filaments connecting the last sarcomeres to the ID (*inset*, *white arrowheads*). Global desmin signal is increased in mutant at D25 (compare *H* to *G*) but desmin tends to accumulate close to the sarcolemma at the periphery of the sarcomeres and ID (*white arrows*) rather than in the center of the myofibrils (*, *inset* in *H*). This phenomenon is amplified at D45 (*I*, *inset*). *Scale bar*, 20 μm.

firmed that the anti-AGE antibody labeled the main desmin spot (Fig. 4*B* and supplemental Fig. S5). Because the increase in desmin-AGE was rather specific among the bands present on the blot, we hypothesized that human desmin, which is conserved from mouse to human, could also be targeted by AGE in human DCM. As a first step in identifying potential alterations of desmin in the context of human heart failure, we examined the pattern of AGE modification in samples of human hearts from patients presenting cardiac dilation (12). Sequential Western blot analysis with the anti-AGE antibody and anti-desmin antibody revealed an increased band with identical apparent M_r as desmin in 6 of 7 patients (Fig. 4*C*) in a similar pattern as observed in SRF^{HKO} mice (Fig. 4*A*).

Recruitment of Phosphorylated αB-crystallin at Deficient Actin Filaments Is Accompanied by a Progressive Disorganization of the Desmin Network—To investigate the subcellular localization of αB-crystallin and desmin in the SRF^{HKO} mutant, we stained heart sections at D25 and D45 with αB-crystallin and desmin antibodies as well as phalloidin to detect polymerized F-actin. Phalloidin signals displayed a progressive decline in cardiomyocytes from D25 to D45 (Fig. 5, *A–F*) in agreement with the data obtained on isolated cardiomyocytes (Fig. 2*B*). Anti-total αB-crystallin antibody displayed a punctiform-striated pattern of expression at the level of the sarcomeres in control cardiomyocytes and labeled the ID (Fig. 5*A*). The αB-crystallin staining increased at D25 and D45 in the SRF^{HKO} mutant when the phalloidin signal progressively declined and the ID became highly stretched and disorganized (Fig. 5, *B* and *C*). At D25, the phospho-Ser^{59} αB-crystallin increased in the SRF^{HKO} at the Z-disk level where it is co-distributed with desmin (Fig. 5, *G* and *H*). Phospho-Ser^{59} and -Ser^{45} αB-crystallin increased at the ID at D25 and at D45 where it colocalized mainly with the remnant of F-actin linking the ultimate sarcomere to the stretched ID (Fig. 5, *E* and *F*, *inset*, *arrowhead*, and supplemental Fig. S6) but also around and between aggregates of desmin at the sarcolemma and ID level (Fig. 5, *H* and *I*, and supplemental Fig. S6). Anti-desmin antibody labeled the cardiomyocytes at the Z-disks, costameres, and ID in the control (Fig. 5*G*). From D25 to D45, desmin staining increased progressively in the SRF^{HKO} in agreement with the two-dimensional DIGE data. The organization of desmin, however, was altered with a trend toward accumulation at the sarcolemma and a progressive loss of the striated pattern, which culminated at D45 (Fig. 5, *H* and *I*,

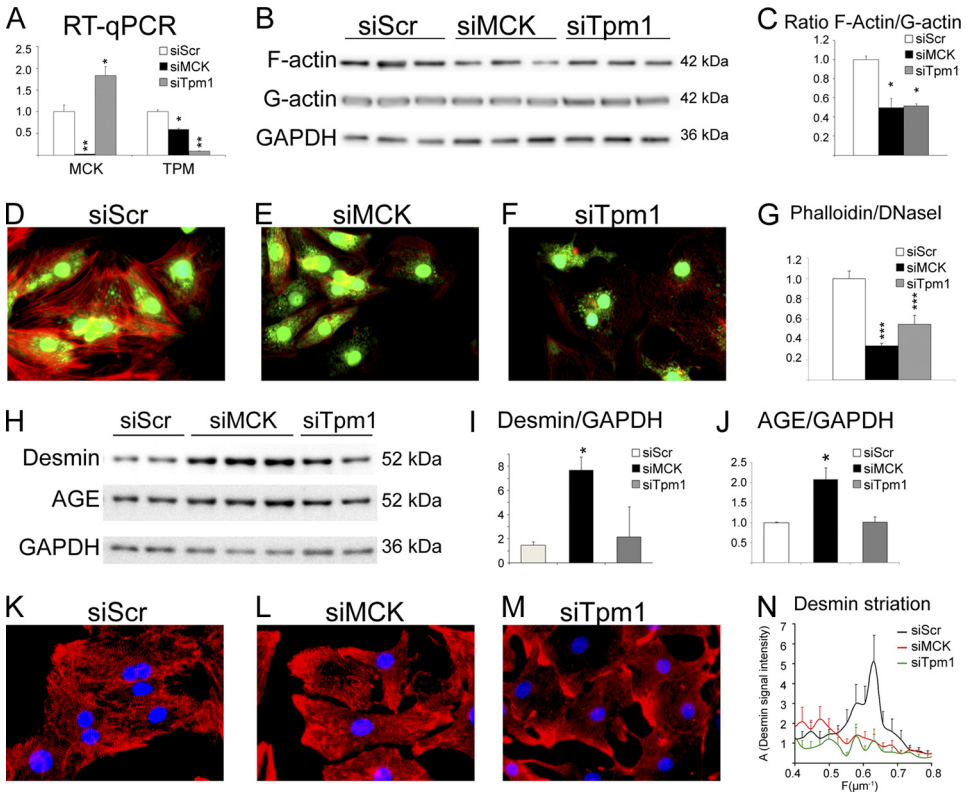

FIGURE 6. **Inhibition of creatine kinase leads to desmin network distribution, actin depolymerization, and AGE formation on desmin.** Neonatal rat cardiomyocytes were transfected at day 5 after plating with siRNA against MCK, tropomyosin (*Tpm1*), or scramble sequence (*Scr*) as a control. Analyses were performed at day 8 of culture. *A*, analysis of mRNA expression of siRNA target by quantitative RT-PCR. *B*, Western blot analysis with anti-sarcomeric α-actin and GAPDH antibodies in the insoluble *versus* the soluble fraction and (*C*) quantification of the actin F/G ratio from Western blot. *D–F*, fluorescence staining for F-actin (phalloidin-TRITC), G-actin (DNase I-Alexa 488), and nucleus (Hoechst). *G*, quantification of the phalloidin and DNase I signal integrate density as measured on individual cardiomyocytes ($n > 40$). *H*, Western blot analysis with anti-desmin, -AGE, and -GAPDH antibodies; and *I* and *J*, quantification of desmin and AGE ratio. *K–M*, fluorescence staining for desmin (*red*) and nucleus (Hoechst). *N*, quantification of desmin network striation: mean fast Fourier transform of desmin signal along a central line in the cardiomyocyte gives mean amplitude A as a function of spatial frequency (μm^{-1}). The major peak is centered around 0.62 μm^{-1} (*i.e.* every 1.6 μm). All ratios are expressed as fold-change over mean control value ± S.E. *, $p \leq 0.05$; ***, $p \leq 0.001$.

arrows, sarcolemma; *asterisk*, reduced or absent signal inside the cardiomyocyte in *right insets*). At the level of the ID, the desmin signal appeared fuzzy and less filamentous at D45 (Fig. 5*I* and supplemental Fig. S6).

Knockdown of MCK Expression in Neonatal Rat Cardiomyocytes Recapitulates Major Aspects of the in Vivo SRF^{HKO} Phenotype—To understand the molecular mechanisms underlying the cascade of events going from MCK down-regulation to cytoskeleton disorganization, we addressed the role of the primary SRF target defects in this process using neonatal rat cardiomyocytes (NRC) as an *in vitro* model.

The two-dimensional DIGE experiments (Fig. 1 and supplemental Table S1) showed that MCK was a labile protein that was more quickly and strongly down-regulated than the stable actin protein (Fig. 2*A* and supplemental Table S2). However, polymerization of actin was already affected at D25 (Fig. 2*B*). MCK is structurally coupled to the myofibrils to provide rapid phosphate transfer from mitochondrial CK-derived phosphocreatine to ADP and generate ATP for local consumption by the myosin ATPase. However, ATP is also known to be required for actin polymerization, which in turn could affect desmin. To determine whether there is a direct link between the loss of MCK activity and cytoskeleton disorganization, we knocked down the expression of MCK using a specific siRNA. We validated down-regulation of the gene at the mRNA level (Fig. 6*A*). The down-regulation was corroborated by a 50% loss of total CK activity in siMCK-transfected *versus* scrambled control siRNA-transfected NRC (siMCK, 2157 ± 207 CK IU/g of protein, *versus* scramble siRNA, 3879 ± 129, *p* value = 0.00396), which fit with the proportion of MCK in these neonatal cells. Knockdown of MCK resulted in the loss of F-actin and decreased actin F/G ratio as measured by cell fractionation (Fig. 6, *B* and *C*) and phalloidin/DNase I staining (Fig. 6, *D–G*). At the same time, siMCK triggered an increase of desmin protein that was modified by AGE (Fig. 6, *H–J*). Desmin network was highly disorganized with accumulation at the membrane and loss of striated pattern (Fig. 6. compare *L* to *K*). We performed fast Fourier transform of the desmin signal along a line parallel to the actin myofibrils to obtain an unbiased estimation of the periodicity of desmin striations. In control NRC, the desmin signal presented a peak with maximal amplitude at a mean frequency of 0.6 μm^{-1}, *i.e.* every 1.7 μm, which was in good agreement with the average length of a sarcomere in cardiomyocytes (Fig. 6*N*). This peak disappeared in siMCK-transfected cells.

Treatment of NRCs with β-guanidinopropionic acid, an analog competitor of creatine, which slows down the phosphocreatine shuttle by the CK system, resulted in a similar reduction of polymerized F-actin and increase in formation of AGE adducts on desmin (supplemental Fig. S7). Altogether, these results showed that inhibition of CK activity *in vitro* is sufficient to

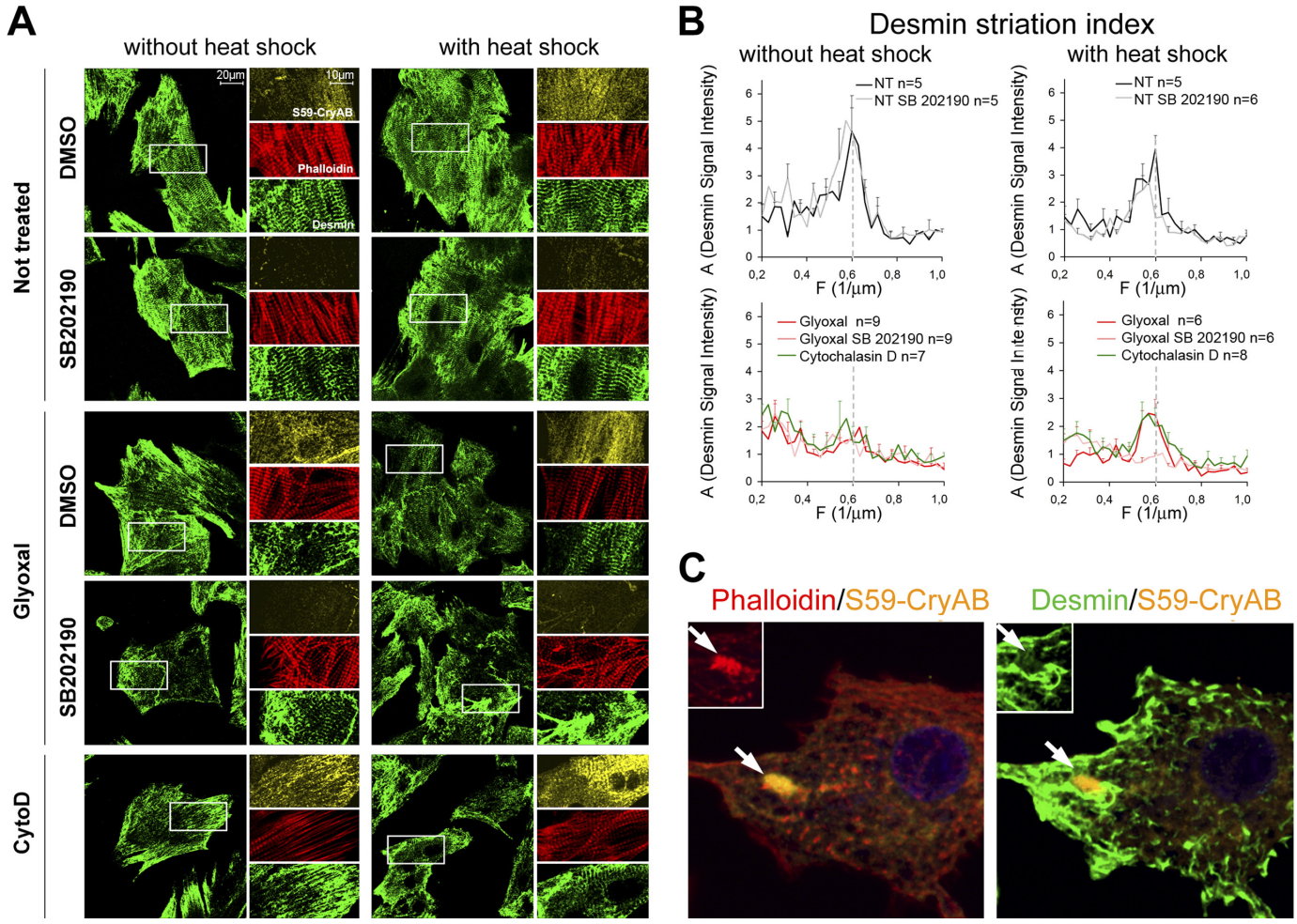

FIGURE 7. **Preactivation of αB-crystallin phosphorylation protects desmin network from short-term treatment with glyoxal or cytochalasin D.** *A*, immunofluorescent co-staining for phospho-Ser^{59} αB-crystallin (*orange*), desmin (*green*), and F-actin (phalloidin-TRITC, *red*). Neonatal rat cardiomyocyte were pre-treated or not by SB202190 (P38 inhibitor) during 6 h, then treated or not by heat shock for 30 min at 42 °C, finally cardiomyocytes were treated by glyoxal or cytochalasin D. *B*, mean fast Fourier transform of the desmin signal along a central line in the cardiomyocyte gives mean amplitude (*A*) as a function of spatial frequency (μm^{-1}). The major peak is centered around 0.6 μm^{-1} (every 1.7 μm). *C*, merged immunofluorescent staining for phospho-Ser^{59} αB-crystallin (*orange*) with F-actin (phalloidin-TRITC, *red* in *left panel*) and desmin (*green* in *right panel*) after 6 h of cytochalasin D treatment. *Arrows* point to the aggregate of phospho-Ser^{59} αB-crystallin (*orange*) that colocalizes with collapsed actin (*red*, *inset in left panel*) but not desmin (*green*, *inset in right panel*).

recapitulate the major characteristics of the SRF^{HKO} phenotype *in vivo*.

Desmin Network Anchorage at the Z-disk of the Sarcomere Is Sensitive to Both Actin Depolymerization and AGE Modification—siRNA-mediated knockdown of MCK altered both actin polymerization and desmin modification by AGE raising the question whether actin depolymerization and/or AGE modification contributed to desmin disorganization. Because α-tropomyosin, which is also down-regulated in the SRF^{HKO} heart, is known to play a role in thin filament stability but unlike MCK, not for energy transfer, we thought to address the consequence of siRNA-mediated knockdown of Tpm1 on actin polymerization and indirectly on desmin organization. siTpm1 triggered a loss of F-actin similar to siMCK in NRC (Fig. 6, *B–G*), whereas it did not affect CK activity (siTpm1 3238 ± 61 CK IU/g of protein, NS *versus* control). siTpm1 also triggered a severe disorganization of desmin network (Fig. 6, *M* and *N*). Because α-tropomyosin is not known to interact directly with desmin, we hypothesize that desmin disorganization is secondary to actin depolymerization. In agreement with this hypothesis, the use of cytochalasin D, an actin depolymerizing agent, was sufficient to trigger desmin disorganization in NRC (Fig. 7*A, bottom panel*, and *B* and *C*).

On the contrary to siMCK, however, siTpm1-induced desmin disorganization did not result in an increase of AGE adduct formation on desmin (Fig. 6, *H–J*). The apparition of AGE modification on desmin protein *in vivo* (Fig. 4) also coincided with the strongest deterioration of desmin filament pattern *in vivo* at D45 (Fig. 5). To investigate whether the AGE modification of desmin could be directly responsible for disorganization of desmin filaments, we treated NRCs with glyoxal, a dicarbonyl precursor of AGE derived from oxidized triose phosphates or lipids, which is naturally present in the cells. The addition of glyoxal to the culture medium for 30 min was sufficient to alter the striated organization of desmin, which accumulated at the membrane. Interestingly, glyoxal did not affect the striated organization of actin suggesting a rather specific effect toward desmin intermediate filaments (Fig. 7*A*, *left panel*). The peak of striated desmin disappeared in glyoxal-treated cells. As mentioned previously, cytochalasin D treat-

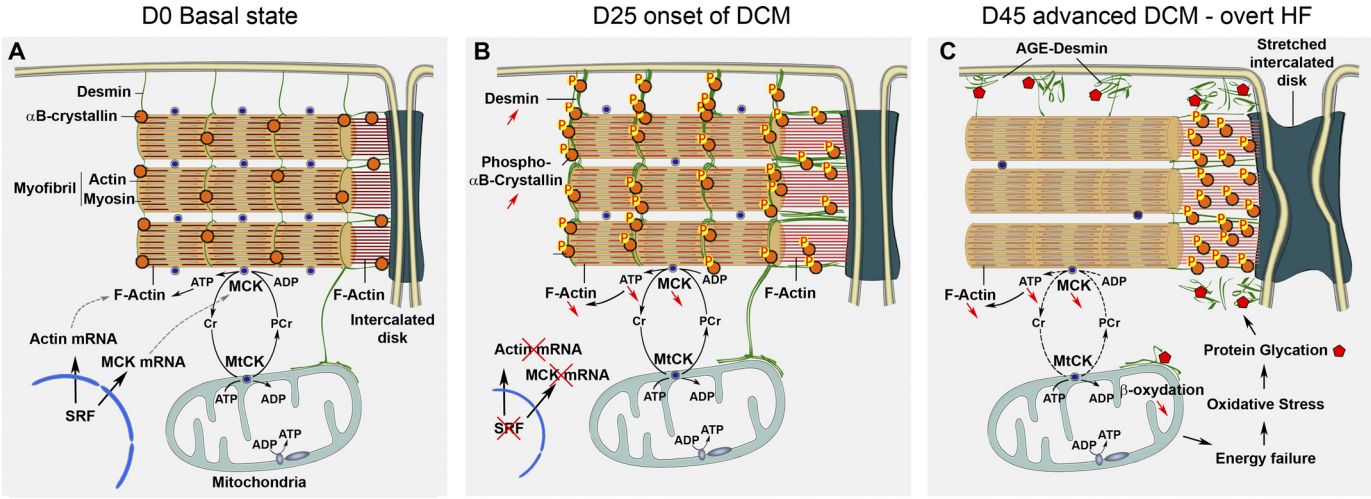

FIGURE 8. **Model for the progressive establishment of DCM and heart failure following SRF inactivation.** *A*, normal molecular cytoarchitecture of a cardiomyocyte in the basal state of the heart. SRF maintains the transcription of genes encoding contractile proteins, sarcomeric α-actin, and MCK. *B*, after 25 days of SRF deletion, cardiac-actin and MCK mRNA are strongly decreased. The more labile MCK protein is decreased and the rapid phosphate transfer from phosphocreatine to ADP is deficient reducing energy delivery to the myofibrillar F-actin. αB-crystallin is phosphorylated and accumulates on actin filaments both in the sarcomere and at the ID. Desmin protein level is increased but maintains its striated pattern and connection to the sarcolemma and ID. *C*, at 45 days, MCK is further down-regulated and enzymes involving fatty acid β-oxidation decrease causing a general energy failure and oxidative stress leading to AGE formation. Desmin is highly sensitive to AGE and the IF network is fragmented with desmin filaments accumulating under the membrane and periphery of the ID. ID is severely stretched and phosphorylated αB-crystallin is essentially recruited on remnants of F-actin linking the last sarcomere to the ID.

ment had as a strong disorganizing effect on desmin (Fig. 7*A*, *bottom panel*). We noticed that glyoxal and cytochalasin D treatment modestly stimulated phosphorylation on serine 59 of αB-crystallin (Fig. 7*A*, compare phospho-Ser^{59} CryAB staining in treated *versus* nontreated cells). To increase αB-crystallin phosphorylation prior to the addition of the drugs, we decided to prime cells by a 30-min heat shock (HS). HS priming increased the signal of phospho-Ser^{59} αB-crystallin compared with unshocked cells and did not affect desmin organization *per se* (Fig. 7*A*, *right panel*). HS priming preserved the striated pattern of desmin in glyoxal and cytochalasin D-treated cells (Fig. 7, *A* and *B*). HS priming also protected the striated pattern of actin filaments from the effect of cytochalasin D (Fig. 7*A*, *lower panel*). The p38 MAPK has been involved in the phosphorylation of serine 59 on αB-crystallin upon most stress signals including vinblastin, cytochalasin D, and HS (22, 23). We show that the p38 MAPK inhibitor SB202190 blocked the appearance of phospho-Ser^{59} αB-crystallin and prevented the protective effect of heat shock against glyoxal, whereas it had no deleterious effect on desmin organization in basal conditions (Fig. 7, *A* and *B*). These results suggest that phospho-Ser^{59} αB-crystallin is potentially able to maintain desmin filament attachment to the sarcomere. However, a longer period of cytochalasin D treatment led to preferential recruitment of phospho-Ser^{59} αB-crystallin on collapsing actin filaments at the exclusion of the desmin network that aggregated on the periphery of collapsed actin and at the cell membrane (Fig. 7*C*). This result explains how a longer period of actin polymerization defect alters the protection of desmin by αB-crystallin.

DISCUSSION

Natural History of DCM following SRF Inactivation—Although different etiologies lead to DCM, this type of cardiac remodeling is characterized by major changes in the cardiomyocytes contractile apparatus and energetic metabolism. Taking advantage of the precise temporal control on pathogenesis provided by inducible Cre-LoxP technology, we carefully analyzed the natural history of the DCM disease and propose the following model. In the basal physiological state, SRF, a transcription factor regulated by important cardiac signaling pathways, maintains a balanced expression of *Ckm* and sarcomeric *Actin* gene expression ensuring the adequacy between phosphocreatine flux and ATP demand by the actomyosin complex (Fig. 8*A*). Following *Srf* inactivation, *Ckm*, *Actin*, and *Tpm1* mRNA are down-regulated but the more labile MCK protein is down-regulated first at the onset of DCM, affecting the ATP-dependent stability of actin filaments that in turn triggers the recruitment of phosphorylated αB-crystallin and an increase of desmin (Fig. 8*B*). With the progression of the disease, further alterations in the thin filament due to down-regulation of actin, tropomyosin, and troponin proteins as well as the complete fall of MCK result in a quasiexclusive recruitment of phosphorylated αB-crystallin at the deficient thin filaments. As a consequence of impaired αB-crystallin protection and increased oxidative stress associated with mitochondrial dysfunctions, desmin is exposed to AGE modifications, which together with the alteration of actin thin filaments, further disrupt the anchorage of desmin intermediate filaments to the sarcomere (Fig. 8*C*).

Importance of MCK Regulation by SRF for Thin Filament Stability—The failing heart is characterized by a metabolic remodeling that includes a fall in CK activity and a decrease of fatty acid oxidation, whereas the potential increase in glucose uptake and utilization driven by the [ADP] and [AMP] increase is not sufficient to compensate for overall decreases in the capacity for ATP supply (3, 20). The reduction of the contractile reserve is also due to alterations in the pool of contractile proteins, through down-regulation of expression, shift of isoforms,

or post-traductional modifications (1). SRF activity is down-regulated in the failing human heart (7, 8) and is repressed by muscle-specific RING finger ubiquitin E3 ligases Murf1 and Murf2, which are activated in heart failure (6, 24). Our study highlights the fact that SRF is an essential co-regulator of the *Ckm* gene and genes encoding sarcomeric proteins in the adult heart as predicted by previous *in vitro* studies (25). Altogether, these studies suggest that deregulation of SRF activity may play an important role in the pathogenesis of heart failure, a hypothesis that will be worth testing in the future on other models of heart failure like experimental infarcts or transverse aortic constriction.

Interestingly, MCK is unique among CK isoforms because it is intimately linked to the myofibrillar compartment and catalyzes the rapid transfer of a phosphate moiety from the mtCK-derived phosphocreatine to ADP, generating ATP right at the site of maximal consumption by the actomyosin complex (26). Here, we show that inhibition of CK-mediated ATP transfer in cultured cardiomyocytes results in a rapid loss of polymerized actin as previously described for other cell types (27, 28) suggesting that early down-regulation of MCK *in vivo* plays a major role in actin filament instability. Although we show that at least one other target of SRF, α-tropomyosin, contributes to the loss of polymerized actin and we cannot exclude that other targets of SRF involved in actin polymerization may have not been detected in the two-dimensional DIGE experiments. The fact that *Ckm* knockout mice display only minor alterations of cardiac parameters in the basal state seems to contradict the apparent importance of MCK down-regulation in the SRF^{HKO} heart (29). However, it should be noted that in MCK knockout mice, the gene product is missing at the beginning of the embryonic development and major adaptative remodeling takes place in this mutant that allows a direct transfer of mitochondria-derived ATP to the myofibrils, including an increased number of mitochondria and a closer interaction of the mitochondria with myofibrils that are thinner than in control mice (30). In the inducible SRF^{HKO} as in the patients experiencing heart failure, the loss of MCK takes place in an adult context in which mitochondrial and myofibrillar networks are already organized in an adult-specific conformation. This hypothesis is in agreement with the idea that reduction of the PCr/ATP ratio is a primary defect in heart failure and is a cause of contractile dysfunction rather than a consequence (31).

Role of αB-crystallin Chaperone Activation in Relationship with Actin and Desmin Filament Organization in DCM—Our results showed that the loss of MCK activity and the subsequent down-regulation of F-actin, triggered a response characterized by phosphorylation of the αB-crystallin chaperone and a striking increase of one of its client proteins, the desmin intermediate filament (Fig. 8*B*). Desmin filaments interconnect myofibrils and mitochondria in the sarcoplasma, and mutations in desmin as well as in αB-crystallin have been directly involved in the development of DCM (32–35). Perturbation of cytoskeletal networks with drugs including cytochalasin D that depolymerizes F-actin, trigger the activation of the p38/MAPKAP2 kinase pathway in a PKA-dependent manner and lead to specific αB-crystallin phosphorylation at serine 59 (22, 23). We found that desmin is stabilized at the post-transcriptional level in the SRF^{HKO} DCM. Phosphorylation of serine 59 on αB-crystallin has been shown to favor actin filament stabilization in H9C2 rat cardiomyocytes (23). Our *in vivo* and *in vitro* analyses are in agreement with a protective role for phosphorylated αB-crystallin for both actin and desmin filament networks, at least in the initial stage of the disease when αB-crystallin co-distributes with both proteins (D25). Heat shock priming, which activates αB-crystallin phosphorylation, protected actin from cytochalasin D-induced disruption but also desmin. HS priming also protected desmin from glyoxal-induced disorganization. When phosphorylation of serine 59 on αB-crystallin was blocked by an inhibitor of the p38 MAPK, which was shown to be upstream of αB-crystallin phosphorylation (22), it suppressed the protective effect of the heat shock. Although p38 MAPK inhibition has certainly a broader impact than simply inhibiting αB-crystallin phosphorylation, we note that it does not impact desmin organization in the basal state. Finally, we showed that upon prolonged cytochalasin D treatment, phosphorylated αB-crystallin was recruited at collapsing F-actin, whereas desmin was excluded from this interaction. Hence, in this specific model of SRF-related DCM, αB-crystallin appears to be able to provide a limited transient protection to the desmin network because it is diverted to deficient actin filaments. This observation raises the hypothesis that the desmin filament network could present a similar defect in other forms of DCM associated to thin filament defect (*e.g.* nemaline myopathy) because of the preferential recruitment of αB-crystallin at the deficient actin filaments.

Desmin Modification by AGE in DCM—We discovered that desmin is a preferential target of AGE in the heart in the SRF-related mouse model of DCM as well as in human patients. Our hypothesis is that alteration of the energy transfer due to the early down-regulation of phosphocreatine shuttle leads to altered mitochondrial functions and increased oxidative stress. Mitochondrial dysfunction and oxidative stress are likely further increased with the down-regulation of mitochondrial enzymes involved in fatty acid β-oxidation and glucose metabolism like the β-enolase at D45. This, in turn, can increase formation of highly reactive dicarbonyls like glyoxal and methylglyoxal coming from triose sugar oxidation or lipid peroxidation and subsequent AGE adduct formation on proteins. The reason why desmin is a preferential target of AGE in the cardiomyocytes remains elusive for now. Partial colocalization of AGE adducts and desmin aggregates was reported in skeletal muscle fibers from patients suffering from desminopathies, suggesting that desmin is prone to AGE adduct modifications in the context of muscle disease (36). Interestingly, vimentin, another type III intermediate filament protein closely related to desmin, is also a preferential target of AGE in the senescent fibroblast where it participates in aggresome formation (37, 38). Desmin and vimentin play an important role in mitochondria distribution in muscle cells and through their interaction with tubulin regulate mitochondrial affinity for ADP, V_{max} of oxygen consumption, and creatine kinase coupling with the adenine nucleotide translocator (39–41). The close vicinity of desmin and mitochondria may explain why desmin is targeted by oxidative stress-derived AGE. We demonstrated that AGE formation on desmin is deleterious for desmin filament network organization. AGE modification of desmin occurs at an intermediate

stage in the establishment of DCM (D45) and we speculate that it plays a role in further deterioration of the cardiomyocyte architecture that takes place in the late stage of the disease between days 50 to 60. AGE-induced disorganization of desmin is likely to create a vicious circle in the course of DCM, aggravating myofibrillar disarray and mitochondrial dysfunction and leading to reduced contractile power and energetic reserve. Hence, it would be interesting in the future to analyze the effect on desmin glycation of a therapeutic compound that inhibits AGE formation, like pyridoxamine, a vitamin B_6 derivative, or Alagebrium (ALT-711), an AGE cross-link breaker (sugar/protein cross-link), which has been used in clinical trials (42, 43). Succeeding to limit AGE formation on desmin in DCM patients may help to preserve cardiac functions. In addition, we note that desmin was also modified by phosphorylation at serine 28. Phosphorylation of several serines at the N terminus head domain of chicken desmin has been shown to inhibit the formation of intermediate filaments (44, 45) and phosphorylated desmin isoforms increase in human myofibrillar myopathies (46, 47). Therefore, the phosphorylation of serine 28 on desmin could be a specific marker of the altered desmin filament network in the context of cardiomyopathy.

Acknowledgments—We thank Prof. Denise Paulin, Dr. Renée Ventura-Clapier, Dr. Anne Garnier, and Dr. Alain Lilienbaum for valuable scientific advice. We thank Dr. Sheila De Souza-Martin for technical help with the two-dimensional Western blot. We thank Philippe Chaffey (Cochin Institute, Paris) for technical help and scientific advice for two-dimensional DIGE experiments. We thank the imaging and animal facilities of IFR83 for expert technical assistance.

REFERENCES

1. Seidman, J. G., and Seidman, C. (2001) *Cell* **104,** 557–567
2. Schmitt, J. P., Kamisago, M., Asahi, M., Li, G. H., Ahmad, F., Mende, U., Kranias, E. G., MacLennan, D. H., Seidman, J. G., and Seidman, C. E. (2003) *Science* **299,** 1410–1413
3. Ventura-Clapier, R., Garnier, A., Veksler, V., and Joubert, F. (2011) *Biochim. Biophys. Acta* **1813,** 1360–1372
4. Miano, J. M. (2010) *Lab. Invest.* **90,** 1274–1284
5. Vartiainen, M. K., Guettler, S., Larijani, B., and Treisman, R. (2007) *Science* **316,** 1749–1752
6. Lange, S., Xiang, F., Yakovenko, A., Vihola, A., Hackman, P., Rostkova, E., Kristensen, J., Brandmeier, B., Franzen, G., Hedberg, B., Gunnarsson, L. G., Hughes, S. M., Marchand, S., Sejersen, T., Richard, I., Edström, L., Ehler, E., Udd, B., and Gautel, M. (2005) *Science* **308,** 1599–1603
7. Davis, F. J., Gupta, M., Pogwizd, S. M., Bacha, E., Jeevanandam, V., and Gupta, M. P. (2002) *Am. J. Physiol. Heart Circ. Physiol.* **282,** H1521–1533
8. Chang, J., Wei, L., Otani, T., Youker, K. A., Entman, M. L., and Schwartz, R. J. (2003) *Circulation* **108,** 407–413
9. Parlakian, A., Charvet, C., Escoubet, B., Mericskay, M., Molkentin, J. D., Gary-Bobo, G., De Windt, L. J., Ludosky, M. A., Paulin, D., Daegelen, D., Tuil, D., and Li, Z. (2005) *Circulation* **112,** 2930–2939
10. Gary-Bobo, G., Parlakian, A., Escoubet, B., Franco, C. A., Clément, S., Bruneval, P., Tuil, D., Daegelen, D., Paulin, D., Li, Z., and Mericskay, M. (2008) *Eur. J. Heart Fail.* **10,** 635–645
11. Sohal, D. S., Nghiem, M., Crackower, M. A., Witt, S. A., Kimball, T. R., Tymitz, K. M., Penninger, J. M., and Molkentin, J. D. (2001) *Circ. Res.* **89,** 20–25
12. Camors, E., Charue, D., Trouvé, P., Monceau, V., Loyer, X., Russo-Marie, F., and Charlemagne, D. (2006) *J. Mol. Cell Cardiol.* **40,** 47–55
13. Gobom, J., Nordhoff, E., Mirgorodskaya, E., Ekman, R., and Roepstorff, P. (1999) *J. Mass Spectrom.* **34,** 105–116
14. Ghelis, T., Bolbach, G., Clodic, G., Habricot, Y., Miginiac, E., Sotta, B., and Jeannette, E. (2008) *Plant Physiol.* **148,** 1668–1680
15. O'Farrell, P. H. (1975) *J. Biol. Chem.* **250,** 4007–4021
16. Larcher, J. C., Boucher, D., Lazereg, S., Gros, F., and Denoulet, P. (1996) *J. Biol. Chem.* **271,** 22117–22124
17. Poggioli, S., Bakala, H., and Friguet, B. (2002) *Exp. Gerontol.* **37,** 1207–1215
18. Verbeke, P., Perichon, M., Borot-Laloi, C., Schaeverbeke, J., and Bakala, H. (1997) *J. Histochem. Cytochem.* **45,** 1059–1068
19. Szweda, L. I., Szweda, P. A., and Holian, A. (2000) *Methods Enzymol.* **319,** 562–570
20. Ingwall, J. S. (2009) *Cardiovasc. Res.* **81,** 412–419
21. Balasubramanian, S., Mani, S. K., Kasiganesan, H., Baicu, C. C., and Kuppuswamy, D. (2010) *PLoS One* **5,** e11470
22. Launay, N., Goudeau, B., Kato, K., Vicart, P., and Lilienbaum, A. (2006) *Exp. Cell Res.* **312,** 3570–3584
23. Singh, B. N., Rao, K. S., Ramakrishna, T., Rangaraj, N., and Rao, ChM. (2007) *J. Mol. Biol.* **366,** 756–767
24. Willis, M. S., Ike, C., Li, L., Wang, D. Z., Glass, D. J., and Patterson, C. (2007) *Circ. Res.* **100,** 456–459
25. Sun, Q., Chen, G., Streb, J. W., Long, X., Yang, Y., Stoeckert, C. J., Jr., and Miano, J. M. (2006) *Genome Res.* **16,** 197–207
26. Ventura-Clapier, R., Kaasik, A., and Veksler, V. (2004) *Mol. Cell Biochem.* **256–257,** 29–41
27. Kuiper, J. W., Pluk, H., Oerlemans, F., van Leeuwen, F. N., de Lange, F., Fransen, J., and Wieringa, B. (2008) *PLoS Biol.* **6,** e51
28. O'Connor, R. S., Steeds, C. M., Wiseman, R. W., and Pavlath, G. K. (2008) *J. Physiol.* **586,** 2841–2853
29. Saupe, K. W., Spindler, M., Tian, R., and Ingwall, J. S. (1998) *Circ. Res.* **82,** 898–907
30. Kaasik, A., Veksler, V., Boehm, E., Novotova, M., Minajeva, A., and Ventura-Clapier, R. (2001) *Circ. Res.* **89,** 153–159
31. Maslov, M. Y., Chacko, V. P., Stuber, M., Moens, A. L., Kass, D. A., Champion, H. C., and Weiss, R. G. (2007) *Am. J. Physiol. Heart Circ. Physiol.* **292,** H387–391
32. Vicart, P., Caron, A., Guicheney, P., Li, Z., Prévost, M. C., Faure, A., Chateau, D., Chapon, F., Tomé, F., Dupret, J. M., Paulin, D., and Fardeau, M. (1998) *Nat. Genet.* **20,** 92–95
33. Goldfarb, L. G., Olivé, M., Vicart, P., and Goebel, H. H. (2008) *Adv. Exp. Med. Biol.* **642,** 131–164
34. Maloyan, A., Osinska, H., Lammerding, J., Lee, R. T., Cingolani, O. H., Kass, D. A., Lorenz, J. N., and Robbins, J. (2009) *Circ. Res.* **104,** 1021–1028
35. Maloyan, A., Sanbe, A., Osinska, H., Westfall, M., Robinson, D., Imahashi, K., Murphy, E., and Robbins, J. (2005) *Circulation* **112,** 3451–3461
36. Janué, A., Odena, M. A., Oliveira, E., Olivé, M., and Ferrer, I. (2007) *J. Neuropathol. Exp. Neurol* **66,** 711–723
37. Ahmed, E. K., Rogowska-Wrzesinska, A., Roepstorff, P., Bulteau, A. L., and Friguet, B. (2010) *Aging Cell* **9,** 252–272
38. Kueper, T., Grune, T., Prahl, S., Lenz, H., Welge, V., Biernoth, T., Vogt, Y., Muhr, G. M., Gaemlich, A., Jung, T., Boemke, G., Elsässer, H. P., Wittern, K. P., Wenck, H., Stäb, F., and Blatt, T. (2007) *J. Biol. Chem.* **282,** 23427–23436
39. Capetanaki, Y. (2002) *Trends Cardiovasc. Med.* **12,** 339–348
40. Kay, L., Li, Z., Mericskay, M., Olivares, J., Tranqui, L., Fontaine, E., Tiivel, T., Sikk, P., Kaambre, T., Samuel, J. L., Rappaport, L., Usson, Y., Leverve, X., Paulin, D., and Saks, V. A. (1997) *Biochim. Biophys. Acta* **1322,** 41–59
41. Tang, H. L., Lung, H. L., Wu, K. C., Le, A. H., Tang, H. M., and Fung, M. C. (2008) *Biochem. J.* **410,** 141–146
42. Little, W. C., Zile, M. R., Kitzman, D. W., Hundley, W. G., O'Brien, T. X., and Degroof, R. C. (2005) *J. Card. Fail.* **11,** 191–195
43. Voziyan, P. A., and Hudson, B. G. (2005) *Cell Mol. Life Sci.* **62,** 1671–1681
44. Geisler, N., and Weber, K. (1988) *EMBO J.* **7,** 15–20
45. Ohtakara, K., Inada, H., Goto, H., Taki, W., Manser, E., Lim, L., Izawa, I., and Inagaki, M. (2000) *Biochem. Biophys. Res. Commun.* **272,** 712–716
46. Caron, A., and Chapon, F. (1999) *Muscle Nerve* **22,** 1122–1125
47. Rappaport, L., Contard, F., Samuel, J. L., Delcayre, C., Marotte, F., Tomè, F., and Fardeau, M. (1988) *FEBS Lett.* **231,** 421–425